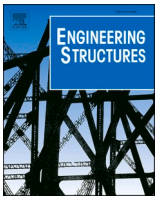
Engineering Structures 276 (2023) 115339



Contents lists available at ScienceDirect

Engineering Structures

journal homepage: www.elsevier.com/locate/engstruct





Design of stainless steel structural systems by GMNIA with strain limits

F. Walport [a,*], H.U. Chan [a], D.A. Nethercot [a], L. Gardner [a]

[a] Department of Civil and Environmental Engineering, Imperial College London, London SW7 2AZ, UK

ARTICLE INFO

Keywords:
Continuous Strength Method
Design by advanced analysis
Global analysis
GMNIA
Inelastic analysis
Local buckling
Stainless steel
Strain limit

ABSTRACT

Design by GMNIA (Geometrically and Materially Nonlinear Analysis with Imperfections) allows the key behavioural features of structures to be directly captured in the analysis, improving accuracy and dramatically reducing the need for subsequent design checks. Since the analysis of frames typically employs beam elements, in which local buckling of cross-sections cannot be explicitly simulated, cross-section classification and capacity checks remain necessary. However, the step-wise and overly conservative nature of these traditional checks restricts accuracy. To resolve this, the use of strain limits, defined using the Continuous Strength Method, in place of these cross-section checks has been proposed. This design method is extended to indeterminate stainless steel structural systems herein. Ultimate load-carrying capacity predictions from the proposed design approach are compared against results obtained from benchmark shell finite element models as well as predictions using traditional stainless steel design methods. The new design framework allows for element interaction at the cross-section level, the influence of local moment gradients, the partial spread of plasticity, moment redistribution, strain hardening and the visualisation of the structural failure mechanism, resulting in more accurate and consistent resistance predictions. The method is included in AISC 370 and prEN 1993-1-14 offering a step change in efficiency for the future direction of structural stainless steel design.

1. Introduction

The most accurate representation of the behaviour of a structure is achieved by directly allowing for instability, plasticity, residual stresses and initial geometric imperfections through the use of a geometrically and materially nonlinear analysis with imperfections (GMNIA) – also referred to as second order or advanced inelastic analysis [1–3]. However, frame analysis is generally carried out using beam finite elements, in which local buckling is not captured, and cross-section classification and cross-section resistance remain necessary. To resolve the step-wise nature and limitations [4] of these traditional checks, use of strain limits, defined using the Continuous Strength Method [5,6], has been proposed [4,7–10]. Unlike the traditional design provisions, application of these strain limits (1) captures the continuous relationship between deformation capacity and full cross-section slenderness, accounting for the beneficial effect of element interaction [11], (2) enables a rational exploitation of the spread of plasticity and strain hardening, which is particularly significant for optimum stainless steel design [12] and (3) allows for the beneficial effects of local moment gradients on cross-section stability [13,14], through strain averaging over the elastic local buckling half-wavelength [15]. Allowance for the interaction between bending moment, shear and torsion [4,7] is made through the use of reduced strain limits. Additionally, at the system level, the strain limits also enable moment redistribution due to plastification to be systematically exploited [8]; an assessment of the design framework for indeterminate stainless steel structures is the focus of the present study.

The described design framework now features in the AISC Design Guide for Structural Stainless Steel (2022) [16], the AISC Specification AISC 370 [17] for the design of hot-rolled and welded stainless steel structures and the draft European Standard prEN 1993-1-14 [18] for the design of steel structures by finite element analysis; inclusion of these new provisions for advanced analysis represents a huge opportunity for enabling more streamlined and efficient design. To date, the accuracy of the design approach for stainless steel has been comprehensively demonstrated for isolated stainless steel members [9]. With a focus on welded I-section continuous beams and single storey portal frames under a variety of loading conditions, comparisons are made herein between the capacity predictions obtained from the GMNIA + CSM design framework and those from benchmark shell finite element models, as well as the conventional EN 1993-1-4 [19] design methods.

* Corresponding author.
E-mail addresses: fiona.walport@imperial.ac.uk (F. Walport), hou.chan19@imperial.ac.uk (H.U. Chan), d.nethercot@imperial.ac.uk (D.A. Nethercot), leroy.gardner@imperial.ac.uk (L. Gardner).

https://doi.org/10.1016/j.engstruct.2022.115339

Available online 14 December 2022
0141-0296/© 2022 The Author(s). Published by Elsevier Ltd. This is an open access article under the CC BY license (http://creativecommons.org/licenses/by/4.0/).

The benchmark shell finite element modelling approach is first set out in Section 2, followed by a summary of the GMNIA + CSM design framework. Section 4 presents the application and assessment of the combined use of beam finite elements and strain limits compared against the results generated using shell finite elements, while Section 5 presents a system reliability analysis to determine the required partial safety factors for use in conjunction with the developed design approach. Finally, a worked example is presented followed by the overall conclusions.

2. Benchmark shell finite element modelling

Benchmark shell finite element (FE) models developed using the general purpose FE software Abaqus [20] are used in this study to assess the accuracy of the GMNIA + CSM design framework. The general modelling approach and validation of the established FE shell models for simulating indeterminate structural stainless steel systems are presented in this section, while the results are utilised in Section 5.

2.1. Modelling approach

Geometrically and materially nonlinear analyses with imperfections (GMNIA) are performed herein using shell elements to generate benchmark data that closely replicate the true behaviour of indeterminate structures. FE models of welded I-section continuous beams and frames are created and the general modelling approach is described in the present sub-section. The 4-noded general purpose S4R [20] shell element with reduced integration has been successfully employed for similar applications in previous studies [21–24] and is also adopted in the present investigation. To define the required pattern of residual stresses and to capture accurately the spread of plasticity and local buckling of the modelled cross-sections, the narrower of the flange and web plate was discretised using 12 elements across the width, with the mesh in the other plates and along the member length defined such that the element aspect ratio was close to unity.

Fixed support conditions were modelled by restraining all degrees of freedom of the nodes at the supported end while pin/roller support conditions were achieved by specifying the relevant boundary conditions at the centre of the cross-section. Web stiffeners (with equal thickness to the web) were included at the locations of pin/roller supports and concentrated loads to prevent web crushing and attached to the cross-section using *MPC, TIE constraints [20] to mimic welded connections. This is analogous to the node coupling approach adopted in [7,25].

The mesh of the column at the column-beam joint region of the modelled frames was generated such that it aligned with the mesh of the beam, with the nodes at the column flange connected to the corresponding nodes at the beam end by *MPC, BEAM constraints [20]. Additional horizontal and diagonal stiffeners were incorporated to facilitate full moment transfer and avoid local failure at the joints, as shown in Fig. 1.

The rounded stress–strain relationship of stainless steel was represented by the two-stage Ramberg–Osgood model [26–28] as given by Eq. (1), and incorporated into the FE models by means of a multi-linear approximation characterised by 135 intervals. The engineering stress–strain curves were transformed to true stress-plastic strain relationships for input into Abaqus. The Poisson's ratio was taken as $\upsilon = 0.3$ in the elastic range and $\upsilon = 0.5$ in the plastic range.

$$\varepsilon = \begin{cases} \dfrac{\sigma}{E} + 0.002\left(\dfrac{\sigma}{f_y}\right)^n & \sigma \leqslant f_y \\ \varepsilon_{0.2} + \dfrac{\sigma - f_y}{E_{0.2}} + \left(\varepsilon_u - \varepsilon_{0.2} - \dfrac{f_u - f_y}{E_{0.2}}\right)\left(\dfrac{\sigma - f_y}{f_u - f_y}\right)^m & f_y < \sigma \leqslant f_u \end{cases} \quad (1)$$

where σ and ε are the engineering stress and strain, E is the Young's modulus, $E_{0.2}$ and $\varepsilon_{0.2}$ are the tangent modulus and total strain at the 0.2% proof stress f_y [28], respectively, f_u is the ultimate tensile stress, ε_u is the ultimate strain, and n and m are the strain hardening exponents.

Both initial geometric imperfections and residual stresses were directly modelled in the benchmark shell FE models to capture their effect on the structural response. Residual stresses were explicitly considered by introducing an initial stress condition, with corresponding residual plastic strains [29], based on the residual stress distribution proposed by Yuan et al. [30] for stainless steel welded I-sections. An additional analysis step prior to the application of load was included for the residual stresses to equilibrate.

At the cross-section level, local sinusoidal plate imperfections were incorporated into the models with amplitudes of $\Delta_{flange} = b/125$ and $\Delta_{web} = h_w/250$, where b is the full flange width and h_w is the web depth.

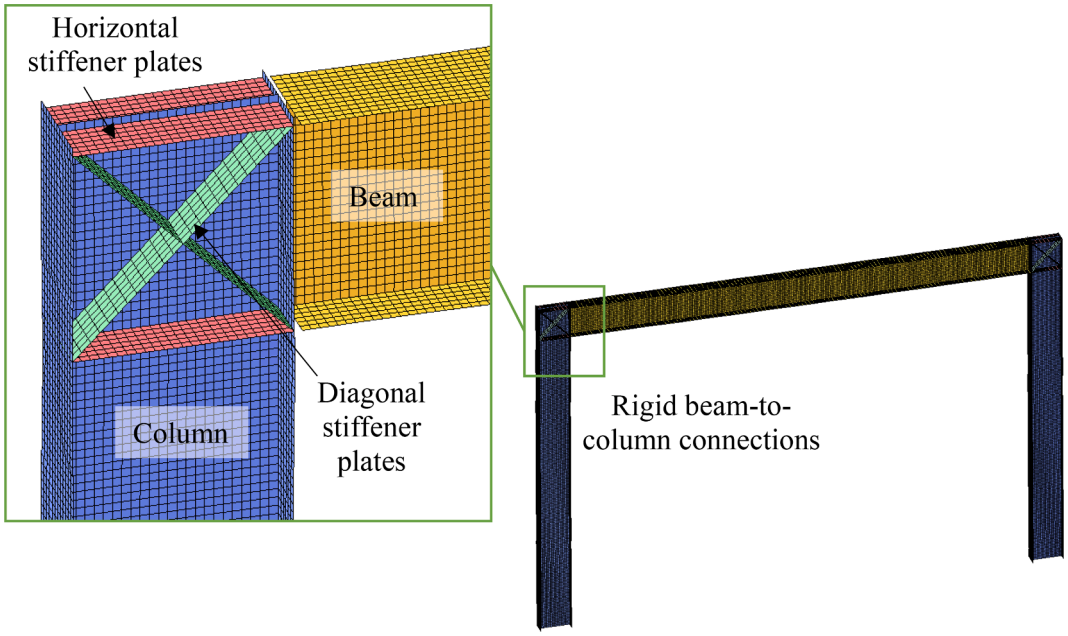


Fig. 1. Modelling of the fully rigid beam-to-column connections in the benchmark shell FE models.

These local imperfection amplitudes (Δ_{flange} and Δ_{web}) correspond to 80% of the fabrication tolerances specified in EN 1090–2 [31], as recommended in prEN 1993-1-14 [18]. The number of sinusoidal waves along each member was defined as the nearest integer number of local buckling half-wavelengths $L_{b,cs}$ that could fit within the member length [7,32], with $L_{b,cs}$ determined from the expressions in [15] assuming pure bending and pure compressive stress distributions in the continuous beam and frame models, respectively. At the member level, an out-of-straightness in the form of a half-sine wave with an amplitude of $L/1000$, where L is the member length, was introduced in the critical direction. At the frame level, all columns were assigned a global sway imperfection in the direction of the horizontal loading with a slope of $\phi = 1/400$ [33,34].

2.2. Validation

To assess the accuracy of the benchmark models, the developed shell FE models were validated against experimental results on 13 austenitic and duplex stainless steel I-section 2-span continuous beams [35,36]. Two load configurations were considered as well as a range of cross-sections with varying slenderness. To replicate the behaviour of the pin/roller supports in the test setup, the relevant boundary conditions were applied to the bottom flange. The measured cross-section geometry, material properties and local and member imperfection amplitudes were used as input parameters for the FE models. Note that where no measured imperfection amplitudes were reported, the amplitudes presented in Section 2.1 were assumed. Where reported, the web and flanges of the welded I-sections were assigned different material properties. All the tests were performed on welded I-sections and thus residual stresses were explicitly introduced using the distribution discussed in Section 2.1.

The welds between the flanges and web of the modelled I-sections were simulated by increasing the thickness of two elements at the web-flange intersections [37]. The thicknesses of these elements were defined such that the cross-sectional areas in the shell FE models and physical tests were the same. Note that the weld dimensions were not reported in [36] and therefore a value of 4 mm was assumed for the corresponding tests.

A summary of the mean and coefficient of variation (CoV) of the shell FE-to-test failure load ratios is provided in Table 1. Note that for the tests in which the ultimate load was not reached due to experimental limitations, the failure load ratio was calculated based on the maximum load attained in the test and the load achieved in the FE model at the same level of deformation (i.e. end rotation or midspan deflection). It can be seen that the shell FE models were able to accurately predict the ultimate loads of the continuous beams, with an overall mean FE-to-test failure ratio and CoV of 0.99 and 0.023, respectively.

Typical load-deformation curves for the 2-span continuous beams subjected to five-point bending with loads applied at the middle of each span presented in [35] are shown in Fig. 2, alongside the corresponding FE curves. Close agreement between the predicted and experimental structural responses was achieved, and it can thus be concluded that the key structural phenomena, including moment redistribution, was accurately captured by the FE models. Therefore, the developed shell FE models are capable of generating reliable benchmark results for indeterminate systems against which the adequacy of the GMNIA + CSM strain limit design method, described in the following section, can be assessed.

Table 1
Summary of shell FE model validation, with a comparison of the experimental and numerical ultimate capacities (FE/Test) for 13 stainless steel I-section continuous beams.

Reference	Stainless steel grade	Load configuration	No. of tests	FE/Test	
				Mean	CoV
Theofanous et al. [35]	Duplex	1/2 span	4	1.01	0.056
	Duplex	1/3 span	4	1.02	0.044
Chen et al. [36]	Austenitic	1/2 span	3	0.97	0.008
	Duplex	1/2 span	2	0.95	0.002
		Total	13	0.99	0.047

3. Design by GMNIA using beam finite elements with strain limits

In this section, the method of design by geometrically and materially nonlinear analysis using beam finite elements with CSM strain limits is outlined. This method is due to be included in the upcoming European Standard prEN 1993-1-14 [18] for the design of steel structures by finite element analysis and has been included in the AISC Specification AISC 370 [17] for the design of hot-rolled and welded stainless steel structures.

3.1. CSM strain limits

3.1.1. Determination of limiting strain ε_{csm}

Since beam elements do not capture the local buckling of cross-sections, additional capacity checks are required. Traditionally, cross-section classification and resistance checks are performed. In the CSM, strain-based checks are calculated. Specifically, the design value of the maximum longitudinal compressive strain ε_{Ed} at each cross-section must satisfy Eq. (2), where ε_{csm} is the CSM compressive strain limit that defines the maximum strain that a cross-section can endure prior to failure, determined from the CSM base curve [5]. The key steps for calculating the CSM limiting strain are detailed in this section.

$$\frac{\varepsilon_{Ed}}{\varepsilon_{csm}} \leqslant 1.0 \tag{2}$$

The CSM base curve defines a relationship between the normalised CSM limiting strain $\varepsilon_{csm}/\varepsilon_y$, where $\varepsilon_y = f_y/E$ is the yield strain, with f_y being the yield (0.2% proof) stress and E being the Young's modulus, and the local slenderness of the full cross-section $\bar{\lambda}_p$, as defined by Eq. (3):

$$\bar{\lambda}_p = \sqrt{\frac{f_y}{\sigma_{cr,cs}}} \tag{3}$$

where $\sigma_{cr,cs}$ is the elastic local buckling stress of the full cross-section, for which simplified formulae are provided in [11].

The CSM base curve is expressed through Eqs. (4) and (5) [9] for non-slender ($\bar{\lambda}_p \leq 0.68$) and slender ($0.68 < \bar{\lambda}_p \leq 1.0$) cross-sections, respectively, where ε_u is the ultimate strain, σ is the maximum compressive stress, n is the strain hardening exponent and Ω is a project specific design parameter defining the permissible level of plastic deformation, with a recommended value of 15.

$$\frac{\varepsilon_{csm}}{\varepsilon_y} = \frac{0.25}{\bar{\lambda}_p^{3.6}} + \frac{0.002}{\varepsilon_y} \quad \text{but} \quad \frac{\varepsilon_{csm}}{\varepsilon_y} \leqslant \Omega \quad \text{for} \quad \bar{\lambda}_p \leqslant 0.68 \tag{4}$$

$$\frac{\varepsilon_{csm}}{\varepsilon_y} = \left(1 - \frac{0.222}{\bar{\lambda}_p^{1.05}}\right)\frac{1}{\bar{\lambda}_p^{1.05}} + \frac{0.002\left(\sigma/f_y\right)^n}{\varepsilon_y} \quad \text{for } 0.68 < \bar{\lambda}_p \leqslant 1.0 \tag{5}$$

3.1.2. Influence of shear

In cases of high shear force, consideration should be given to the adverse influence on the bending capacity. In the CSM, the influence of high shear, and its interaction with co-existing bending moment, is accounted for through the definition of a reduced strain limit $\varepsilon_{csm,V}$. Shear capacity checks (including shear buckling where necessary) should also be performed using the relevant provisions of EN 1993-1-1 [38] and EN 1993-1-5 [39]. Full details for these provisions are given in [4], as included in prEN 1993-1-14 [18].

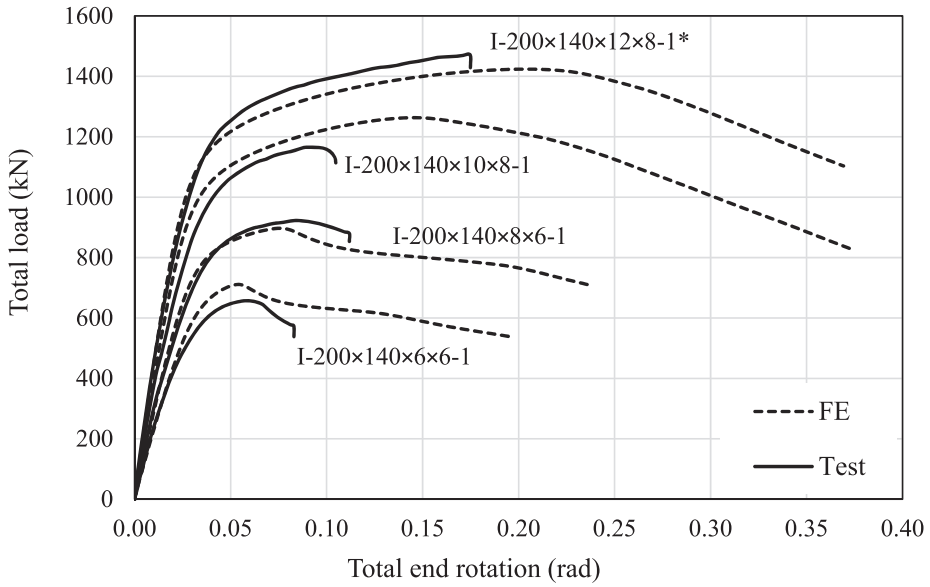


Fig. 2. Validation of the shell FE model against five-point bending test results with mid-span concentrated loads reported in [35]. Note that the * symbol indicates a test where the ultimate load was not achieved due to excessive deformation.

3.1.3. *Elastic local buckling half-wavelength*

To capture the beneficial effect of local bending moment gradients on the local stability of cross-sections, the compressive strains may be averaged over the corresponding local buckling half-wavelength $L_{b,cs}$ for each considered cross-section [7]. The elastic local buckling half-wavelength $L_{b,cs}$ can be obtained numerically [40] or through explicit formulae [15] based on the first-order internal force distribution.

3.2. *Beam finite element modelling*

The studied design method (GMNIA + CSM strain limits) is implemented by means of beam finite element modelling. The beam finite element models are developed herein using the finite element software Abaqus [20], with the linear Timoshenko B31OS beam element used in all simulations. The mesh size was chosen to ensure that the deformed shape of the examined systems and the spread of plasticity was accurately captured along the member length; note that, as a minimum requirement, the elements should have a length less than or equal to the corresponding local buckling half-wavelength $L_{b,cs}$, as discussed in Section 3.1.3. A sufficient number of section points was assigned along each flange and web plate to ensure that the spread of plasticity was accurately captured throughout the cross-section; 33 sections points were employed herein.

The influence of the material nonlinearity is directly modelled through the definition of the full stainless steel stress–strain curve using the two-stage Ramberg–Osgood model [28], as further detailed in Section 2.1, and incorporated into the beam FE models in true stress (σ_{true})-plastic strain (ε^{pl}_{true}) form. Note that in Abaqus, while the default value of the effective (plastic) Poisson's ratio in shell elements is 0.5, for beam elements this default value is 0; therefore, a value of 0.5 was explicitly defined. For the purposes of design by GMNIA, all material and geometric properties should be taken as the nominal values, except for the Young's modulus, where a reduced value, equal to $E = 191000$ N/mm^2 for stainless steel, is recommended [41]. This is particularly important in stability governed scenarios, such as frames with slender compression members.

Account should be taken of both initial geometric imperfections and residual stresses. The CSM strain limits include the influence of initial geometric imperfections and residual stresses at the local cross-section level. At member level, geometric bow imperfections and residual stresses can be considered separately. However, for ease of design, equivalent bow imperfections [41], as calculated using Eq. (6) and included in prEN 1993-1-14 [18], may be modelled in the analysis to allow for the combined effect of geometric imperfections and residual stresses. The imperfections may be applied either by direct modelling as a half-sine wave or through scaling of a suitable elastic buckling mode.

$$e_0 = \frac{\alpha L}{150} \quad \text{but} \quad e_0 \geqslant \frac{L}{1000} \tag{6}$$

where L is the member length and α is the imperfection factor [42].

Equivalent frame out-of-plumbness amplitudes for use in design by GMNIA have yet to be developed and, therefore, the geometric sway imperfection for elastic analysis with an elastic cross-section verification (as opposed to the frame imperfections for use with a plastic cross-section verification, which would be overly conservative since plasticity is captured in analysis) is used herein with a slope of $\phi = 1/400$ [18,33].

3.3. *Direct resistance check*

The ultimate resistance determined from the GMNIA R_{GMNIA} is the first to occur of (1) the peak load, after which the load-deformation response decreases or (2) the load at which the average strain over the cross-section elastic local buckling half-wavelength reaches the corresponding CSM limit strain. These correspond to the two criteria C1 and C2 defined in prEN 1993-1-14 [18].

Owing to the incremental nature of nonlinear analyses, the exact point at which the strain limit is achieved will not match the obtained solution points precisely; interpolation should therefore be used between the load levels either side of the point at which Eq. (2) is satisfied. It should be noted though that, with sufficiently fine load increments, this discrepancy is usually very small.

The characteristic resistance $R_{b,k}$, given by Eq. (7), corresponds to the load level at which the peak load or CSM strain limit is first reached R_{GMNIA}, divided by γ_{FE}, where γ_{FE} is the model factor that accounts for the uncertainties of the numerical model, as discussed in Section 3.4.

$$R_{b,k} = \frac{R_{GMNIA}}{\gamma_{FE}} \tag{7}$$

Finally, the design resistance $R_{b,d}$ is determined from Eq. (8), where γ_{Mi} is the partial factor for the relevant failure mode according to EN 1990 [43] and the relevant parts of EN 1993. For the resistance of

members to instability, the partial factor γ_{M1} is utilised, with a value of 1.1 for stainless steel [42].

$$R_{b,d} = \frac{R_{b,k}}{\gamma_{Mi}} \tag{8}$$

3.4. Calculation of model factor

The described design method (i.e. GMNIA + CSM strain limits) is underpinned by beam finite element modelling. Therefore, the uncertainty associated with the adopted beam FE models will have a direct influence on the final design outcomes. This numerical uncertainty is accounted for through the model factor γ_{FE}, which can be determined using Eq. (9) following the general model validation process described in Annex A of prEN 1993-1-14 [18].

$$\gamma_{FE} = \frac{1}{m_x(1 - k_n V_x)} \geqslant 1.0 \tag{9}$$

where m_x and V_x are determined based on validation of the FE models against experiments, and are the average and coefficient of variation of the ratio of the experimental to numerical failure loads, respectively, and k_n is the characteristic fractile factor (assuming an unknown V_x) given in Annex D of EN 1990 [43], which is a function of the number of test results n.

As an illustration of determining γ_{FE}, the beam finite modelling approach employed in the presented design method is applied here to the same continuous beam tests utilised in Section 2.2 for the shell finite element model validation. As for the validation of the shell FE models, the measured geometric and material properties were used. To account for the different material properties in the flanges and web, weighted average material properties were employed based on their relative contribution to the cross-section bending capacity, as given for the yield strength $f_{y,av}$ by:

$$f_{y,av} = \frac{2f_{y,f}A_f(h_w/2 + t_f/2) + 2f_{y,w}(A_w/2)(h_w/4)}{W_{pl}} \tag{10}$$

where A_f and A_w are the flange and web areas, respectively, $f_{y,f}$ and $f_{y,w}$ are the flange and web yield strengths, respectively, h_w is the height of the web, t_f is the thickness of the flange and W_{pl} is the plastic section modulus.

The same approach was also used for the weighted average ultimate strength, ultimate strain, and strain hardening exponents n and m.

The failure load of each of the tested continuous beams was predicted by the GMNIA-based design method with CSM strain limits outlined in Section 3. The obtained mean test-to-FE failure load ratio m_x was 1.151 with a corresponding coefficient of variation V_x of 0.066. The value of k_n for 13 test specimens (i.e. $n = 13$) is 1.85. Therefore, as calculated below, the γ_{FE} for the beam FE model adopted in the present study is 1.0.

$$\gamma_{FE} = \frac{1}{1.151(1 - 1.85 \times 0.066)} = 0.986 \quad \text{but} \quad \gamma_{FE} \geqslant 1.0, \quad \text{hence} \quad \gamma_{FE} = 1.0 \tag{11}$$

4. Application and assessment of GMNIA-based design method with CSM strain limits

The accuracy of the presented GMNIA-based design method using beam elements with strain limits is assessed in this section for a range of stainless steel I-section indeterminate structural systems. The results are compared against the benchmark ultimate loads determined using the shell FE models α_{shell} described in Section 2.1. Comparisons are also made against the results obtained using traditional design calculations according to EN 1993-1-4 [19], with all partial factors set to unity. The material properties for the most widely used austenitic (1.4301), duplex (1.4362) and ferritic (1.4510) stainless steels were employed [44], as summarised in Table 2 [45,46]. Two-span (CB-LC1) and three-span (CB-LC2, CB-LC3) continuous beams were assessed, as well as single span portal frames under five load cases (F-LC1, F-LC2, F-LC3, F-LC4, F-LC5); an overview of the considered loading configurations and varied parameters are given in Table 3.

Table 2
Nominal (cold rolled strip [45]) and mean material properties assumed herein for three common stainless steel grades [44,46].

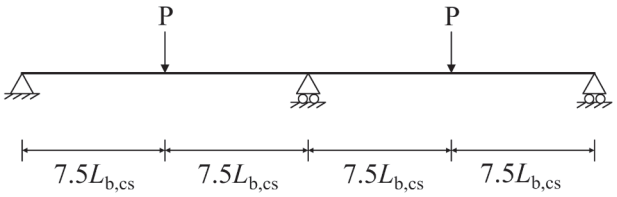
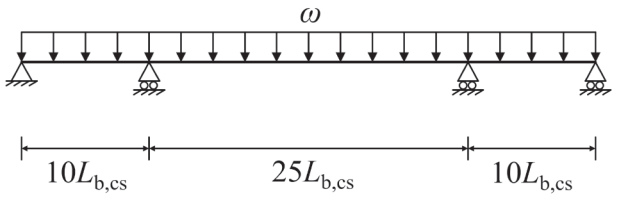
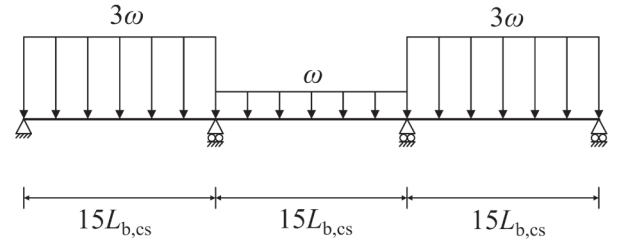
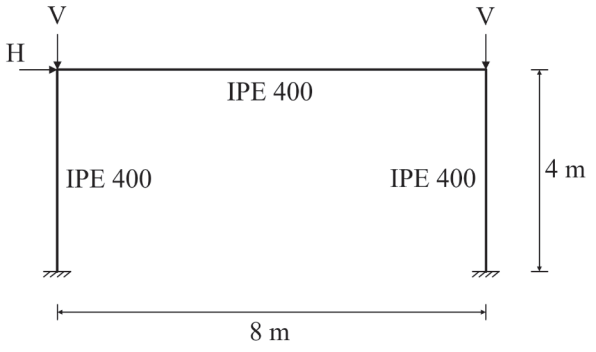
Stainless steel grade	Statistical value	E (N/mm^2)	f_y (N/mm^2)	f_u (N/mm^2)	n	m	ε_u
Austenitic (1.4301)	Nominal	191,000	230	540	9.1	2.3	0.5
	Mean	200,000	287.5	594			
Duplex (1.4362)	Nominal	191,000	450	650	9.3	3.6	0.3
	Mean	200,000	495	715			
Ferritic (1.4510)	Nominal	191,000	240	420	17.2	2.8	0.16
	Mean	200,000	276	462			

To ensure compatibility between the shell and beam FE models, particular care was taken in modelling the joint regions of the frames, with the joint regions in the beam FE models represented by beam elements with the same stiffness as the corresponding shell benchmark models. This was achieved by calculating the second moment of area based on the compound cross-section (i.e. column plus diagonal stiffeners) in the shell FE model at several locations along the depth and width of the joint region. The cross-section geometries of the beam elements within the joint regions of the beam FE model were then defined such that the respective second moments of areas were achieved, as illustrated in Fig. 3. Note that the cross-sections with second moments of area I_1 and I_6 (see Fig. 3) correspond to the horizontal plate stiffener and the column flange, respectively, and were modelled using B31 [20] beam elements with solid rectangular cross-sections. Weld fillets at the web-flange intersections were not considered in the parametric study.

The normalised capacity predictions α_{ult}/α_{el}, where α_{ult} is the ultimate load factor, as predicted from benchmark shell FE models, beam FE GMNIA + CSM strain limits and traditional EN 1993-1-4 design, and α_{el} is the load factor at which first yield occurs, for the austenitic stainless steel CB-LC1 continuous beams and duplex stainless steel CB-LC2 continuous beams are presented in Figs. 4 and 5, respectively. It should be noted that the normalised EC3 capacity predictions for Class 1 ($\alpha_{coll}/\alpha_{el}$) and Class 2 ($\alpha_{pl}/\alpha_{el}$) cross-sections shown in Figs. 4 and 5, where α_{coll} is the plastic collapse load factor calculated using traditional plastic hinge theory, and α_{pl} is the load factor at which the first plastic hinge forms, are mean values. It can be observed in Figs. 4 and 5 that an increase in the maximum allowable deformation capacity from $\Omega = 15$ to $\Omega = 30$ results in an even closer representation of the shell FE model behaviour. The design predictions become more conservative in the slender range ($\bar{\lambda}_p > 0.68$) since, although some redistribution is captured due to material nonlinearity below the 0.2% proof stress (as described by the Ramberg–Osgood material model), the CSM capacity is defined as the point at which the strain limit is first reached within the structure; in reality, the ultimate load of the system can occur after the first cross-section has deformed beyond its peak capacity and is on the falling branch, while the forces and moments at other locations continue to rise [47,48].

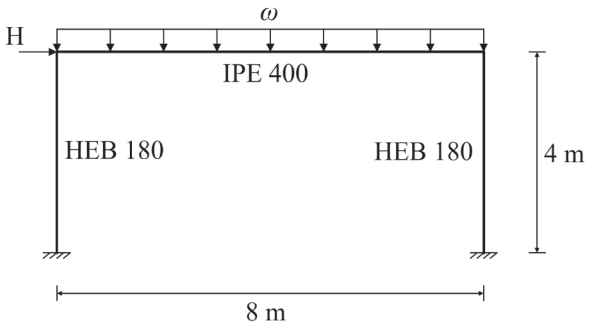
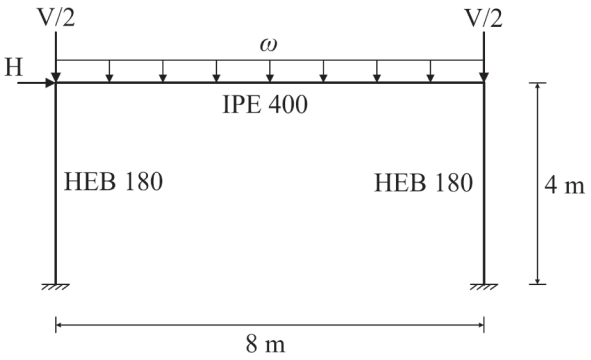
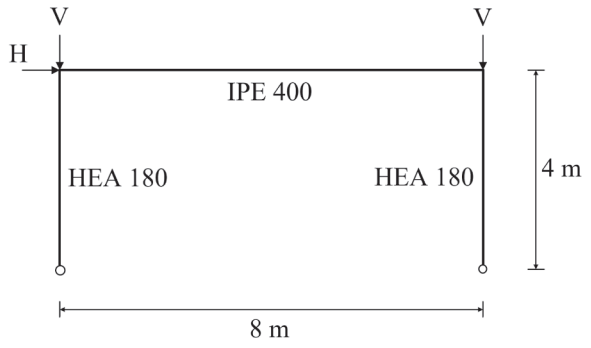
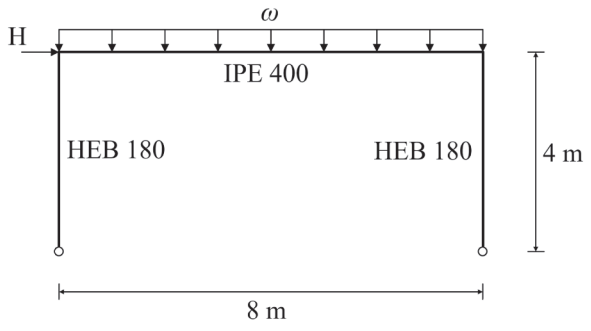
The normalised capacity predictions $\alpha_{ult}/\alpha_{shell}$ for all 225 considered frames are presented in Fig. 6, where α_{ult} is the ultimate load factor, as predicted using beam FE GMNIA + CSM strain limits and EN 1993-1-4 [19]. For EN 1993-1-4, a number of design cases (DC) are assessed, as summarised in Table 4, in which $\varepsilon = \sqrt{235/f_y}$. As concluded in [7–10], the CSM strain limits allow a rational utilisation of the benefits from strain hardening, plastic redistribution and local moment gradients and consequently give close but generally safe-sided predictions of the benchmark shell FE results, with mean and coefficient of variation (CoV) values of the design-to-benchmark FE ultimate capacity ratios of 0.99 and 0.025, respectively. By contrast, it can be observed that the EC3 results are both significantly more conservative and scattered, with

Table 3
Overview of continuous beams and frames considered for each of the three grades of stainless steel during the assessment of the presented method of design by GMNIA with CSM strain limits.

Load case	No.	Varied parameters
CB-LC1: 	40	$0.2 < \bar{\lambda}_p < 1.0$
CB-LC2: 	40	$0.2 < \bar{\lambda}_p < 1.0$
CB-LC3: 	40	$0.2 < \bar{\lambda}_p < 1.0$
F-LC1: 	15	$0 \leq H/2V \leq 1.4$

(*continued on next page*)

Table 3 (*continued*)

F-LC2: 		15	$0 \leq H/8\omega \leq 7$
F-LC3: 		5	H/V = 0.005 $V/8\omega = [1, 2, 3, 4, 5]$
		5	H/V = 0.05 $V/8\omega = [1, 2, 3, 4, 5]$
		5	H/V = 0.1 $V/8\omega = [1, 2, 3, 4, 5]$
F-LC4: 		15	$0 \leq H/2V \leq 1.4$
F-LC5: 		15	$0 \leq H/8\omega \leq 7$

mean and coefficient of variation values of the normalised capacity of 0.83 and 0.106, respectively. All examined EC3 design cases are in accordance with Method M4 of prEN 1993-1-1 [49], based on second order analysis with imperfections; however, two different material models – elastic, perfectly-plastic and Ramberg-Osgood are considered, and varying degrees of plastic redistribution at cross-section and system levels are permitted, depending on the cross-section class - see Table 4. Note that DC 1.1 is used for the frames with Class 1 cross-sections in Fig. 6. The normalised ultimate capacity predictions of the austenitic stainless steel frame cases F-LC2 and F-LC5 are presented in Fig. 7. These frames are formed of Class 1 cross-sections and thus design cases (DC) 1.1, 1.2 and 2 are considered. In DC 1.2 and 2, a cross-section check is used and thus failure is predicted to occur when the first hinge forms. Note that in DC 1.2, the nonlinear (rounded) nature of the Ramberg-

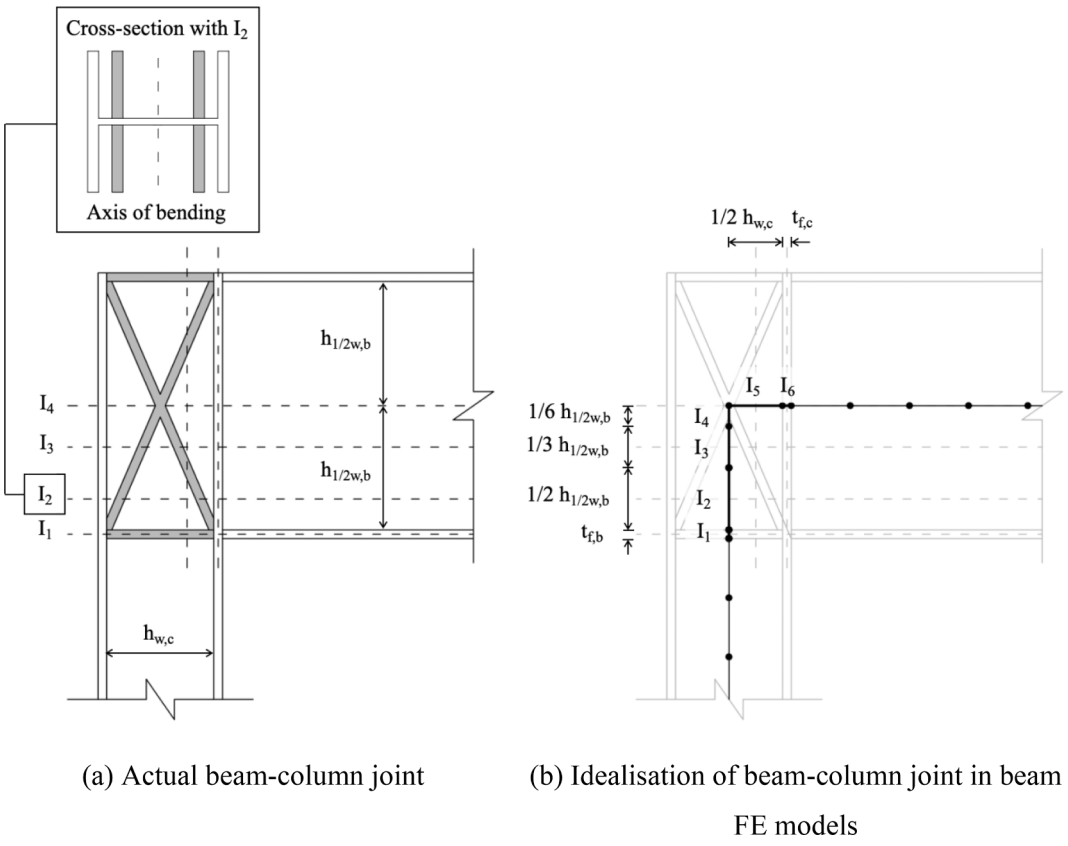


Fig. 3. Modelling of beam-column joint in beam FE models.

Osgood stress–strain curve results in a degree of plastic redistribution prior to the first hinge forming. DC 2 yields overly conservative resistance predictions for frames with Class 1 cross-sections since plastic redistribution is ignored. This conservativism is more significant in F-LC2 than in F-LC5 due to the higher degree of indeterminacy in frames with fixed supports. Of the EC3 design cases, DC 1.1, which allows full plastic redistribution, provides the most accurate resistance predictions. However, the beneficial effects of strain hardening and local moment gradients are not accounted for and therefore the predictions are still overly conservative compared with the benchmark shell results.

In all cases, the presented design framework of geometrically and materially nonlinear analysis with imperfections using beam elements and CSM strain limits provides significantly more accurate and consistent capacity predictions of the benchmark shell FE results than EN

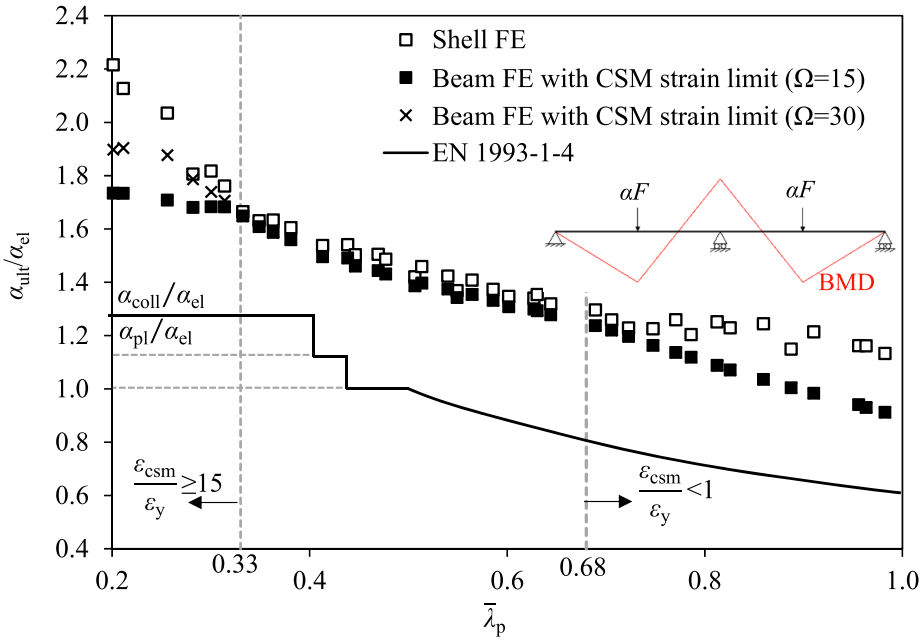


Fig. 4. Normalised capacity predictions for austenitic stainless steel I-sections of varying local cross-section slenderness for CB-LC1.

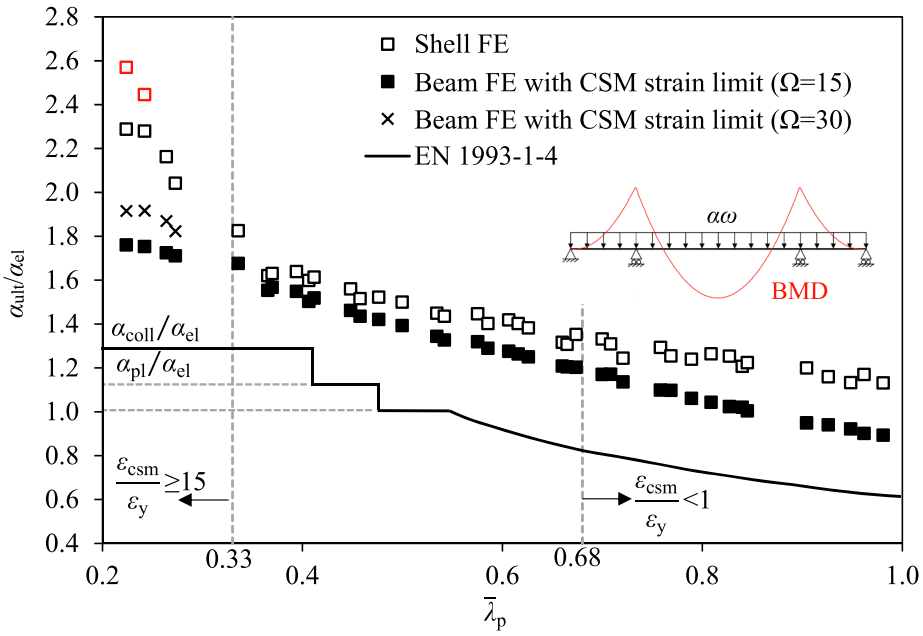


Fig. 5. Normalised capacity predictions for duplex stainless steel I-sections of varying local cross-section slenderness for CB-LC2. Note that the two red squares correspond to the benchmark shell results that were capped (i.e. $\alpha_{shell}/\alpha_{beam} \leq 1.3$) to prevent the reliability analysis being skewed by the excessively conservative results. (For interpretation of the references to colour in this figure legend, the reader is referred to the web version of this article.)

1993-1-4 [19]. The design framework is straightforward and computationally efficient to implement and able to capture the beneficial effects of the spread of plasticity, strain hardening, local moment gradients and the degree of permissible moment redistribution due to plastification and member instability.

5. Reliability analysis

In this section, the reliability of the presented approach for the design of structural stainless steel systems (with Ω set to the default recommended value of 15) is evaluated following the standard procedure set out in EN 1990 Annex D [43] based on the First Order Reliability Method (FORM). An alternative Monte Carlo-based approach [2,50–55] has been used for the system-based reliability analysis of stainless steel frames in [56,57]. In these studies, in addition to the variability of the basic geometric and material properties that are considered herein, the variability of connection stiffness and amplitudes of initial geometric imperfections and residual stresses is also considered.

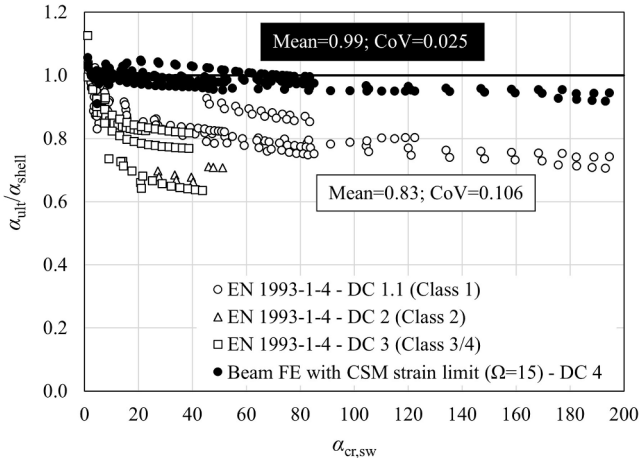


Fig. 6. Normalised capacity predictions for all 225 frames considered (75 frame configurations × 3 stainless steel grades), where $\alpha_{cr,sw}$ is the elastic critical load factor associated with global sway mode calculated for each frame at α_{shell}.

To facilitate the reliability study implemented herein, six analyses were performed for each indeterminate structural system; the six analyses, and their purpose, are defined in Table 5. In line with the provisions of Annex E of prEN 1993-1-1 [49], the mean values of all the geometric properties were taken equal to the nominal values except for the flange thickness t_f, which was taken as 0.98 times the nominal value.

The ratio of the mean to nominal yield strength, referred to as the material over-strength factor, $f_{y,m}/f_{y,n}$ and the corresponding coefficient of variation of the yield strength V_{fy} were taken as 1.25 and 0.07 for austenitic, 1.1 and 0.04 for duplex, and 1.15 and 0.07 for ferritic stainless steel, respectively. The coefficient of variation of the Young's modulus V_E was taken as 0.03 [49] while the coefficient of variation of the cross-sectional area V_A was calculated based on the parameters of the geometric dimensions provided in [49] and following the procedure outlined in [58], resulting in a value of V_A equal to 0.02.

The varying dependence of the resistance of each numerical simulation on the yield stress f_y, cross-sectional area A and Young's modulus E was considered through a combined coefficient of variation V_{rt} as given by Eq. (12), with the participation coefficients [59] C_1, C_2 and C_3 calculated as detailed in [9] using analyses 2–5 in Table 5. Note that it is important to ensure that the analyses are performed with sufficiently small increments to prevent the occurrence of spurious results in the exponent calculations, which can be sensitive to small changes in resistance.

$$V_{rt} = \sqrt{(C_1 V_{fy})^2 + (C_2 V_A)^2 + (C_3 V_E)^2} \tag{12}$$

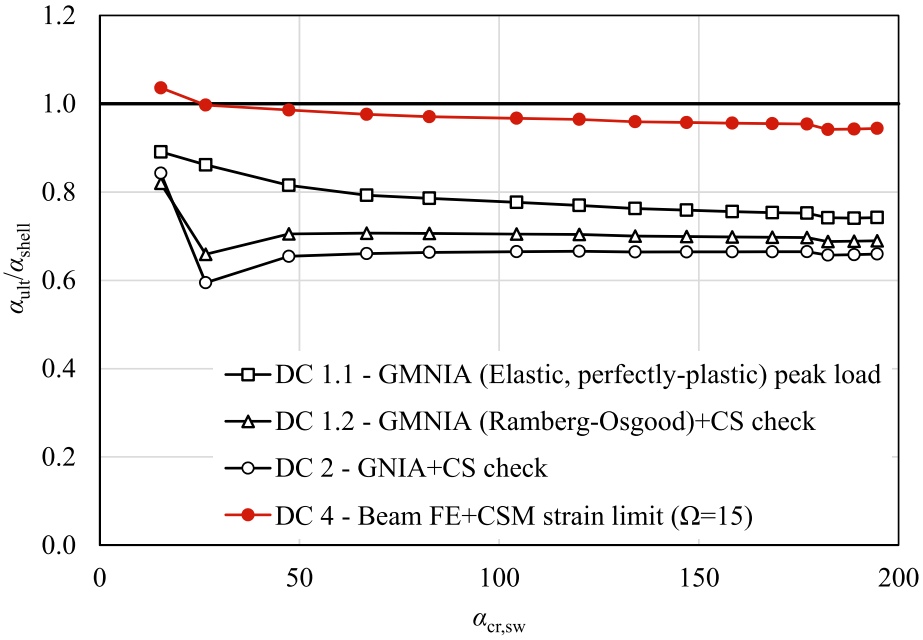
The correction factor b was calculated using Eq. (13) [60], where r_e is the benchmark resistance obtained from the shell FE models, r_t is the predicted resistances obtained from the presented design method (see Table 5) and n is the total number of FE simulations.

$$b = \frac{1}{n}\sum_{i=1}^{n}\frac{r_{e,i}}{r_{t,i}} \tag{13}$$

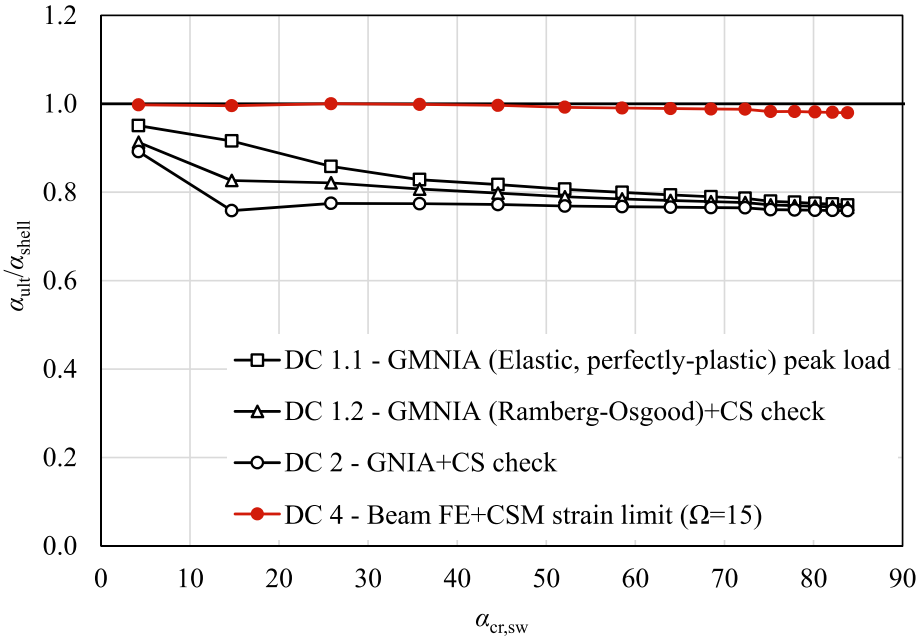
The design fractile factor $k_{d,n}$ and the coefficient of variation of the

Table 4
Summary of the design approaches employed herein for the prediction of the ultimate capacity of the considered frame cases. Design cases 1 to 3 correspond to different Eurocode design cases, while design case 4 corresponds to the presented design framework of beam FE GMNIA with CSM strain limits.

Design Case (DC)	Cross-section class	Analysis	Material model	Imperfection		Failure criteria
				Global	Member	
1.1	1	GMNIA	Elastic, perfectly-plastic	1/400	$\alpha\beta L$ (β=1/150) [18]	Peak load (allowing full plastic redistribution)
1.2	1	GMNIA	Ramberg-Osgood	1/400	$\alpha\beta L$ (β=1/150) [18]	Linear plastic cross-section check
2	1/2	GNIA	N/A	1/200	$\alpha\beta L/\varepsilon$ (β=1/75) [47]	Linear plastic cross-section check
3	3/4	GNIA	N/A	1/400	$\alpha\beta L/\varepsilon$ (β=1/110) [47]	Linear elastic cross-section check
4	N/A	GMNIA	Ramberg-Osgood	1/400	$\alpha\beta L$ (β=1/150) [18]	Peak load / CSM strain limit



(a) F-LC2-Austenitic



(b) F-LC5-Austenitic

Fig. 7. Normalised capacity predictions obtained for the austenitic stainless steel F-LC2 and F-LC5 frames with Class 1 cross-sections for the different EN 1993-1-4 [19] design cases (DC 1.1, DC 1.2, DC 2 and DC 4).

Table 5
The six analyses required for each indeterminate structural system in the reliability assessment according to EN 1990 [43] for design by GMNIA using beam elements with strain limits.

Analysis	Purpose	Model type	Material and geometric properties
1	Benchmark resistance, r_e	Shell	Mean
2	Predicted resistance, r_t	Beam	Mean
3	To determine dependence of resistance on variation in f_y through C_1	Beam	Mean + $1.05f_y$ + $1.05f_u$
4	To determine dependence of resistance on variation in A through C_2	Beam	Mean + $1.05A$
5	To determine dependence of resistance on variation in E through C_3	Beam	Mean + $1.05E$
6	Nominal resistance, r_n	Beam	Nominal

Table 6
Summary of statistical analysis results for presented design method assessed against benchmark shell FE results for austenitic, duplex and ferritic stainless steel I-section continuous beams. Note that the * symbol indicates the cases where some of the results were capped ($b = r_e/r_t \leq 1.3$) to prevent the reliability analysis being skewed by excessively conservative results.

Load case	Grade	Stocky					Intermediate					Slender				
		b	V_δ	V_r	γ^*_{M1}	$\frac{\gamma^*_{M1}}{\gamma_{M1}}$	b	V_δ	V_r	γ^*_{M1}	$\frac{\gamma^*_{M1}}{\gamma_{M1}}$	b	V_δ	V_r	γ^*_{M1}	$\frac{\gamma^*_{M1}}{\gamma_{M1}}$
CB-LC1	Austenitic	1.149	0.083	0.119	1.05	0.95	1.031	0.009	0.071	1.02	0.93	1.145	0.074	0.093	1.05	0.95
	Duplex	1.066	0.023	0.062	1.04	0.95	1.054	0.028	0.057	1.06	0.97	1.207	0.057	0.073	1.01	0.91
	Ferritic	1.171	0.084	0.121	1.11	1.01	1.039	0.028	0.076	1.10	1.00	1.165	0.083	0.100	1.12	1.02
CB-LC2	Austenitic	1.197*	0.098	0.130	1.04	0.95	1.005	0.010	0.072	1.05	0.95	1.101	0.067	0.088	1.07	0.97
	Duplex	1.262*	0.041	0.069	0.90	0.82	1.080	0.021	0.054	1.03	0.93	1.204	0.052	0.069	0.99	0.90
	Ferritic	1.204*	0.091	0.125	1.10	1.00	1.016	0.028	0.076	1.12	1.02	1.115	0.076	0.094	1.14	1.04
CB-LC3	Austenitic	1.180*	0.113	0.137	1.07	0.97	0.994	0.027	0.073	1.07	0.97	1.129	0.067	0.085	1.04	0.95
	Duplex	1.230*	0.045	0.066	0.91	0.83	1.008	0.034	0.035	1.05	0.95	1.174	0.055	0.065	1.01	0.92
	Ferritic	1.193*	0.100	0.126	1.11	1.00	1.017	0.029	0.073	1.11	1.01	1.162	0.072	0.089	1.08	0.98

predicted resistances relative to the benchmark resistances V_δ were calculated according to [43]. Since the standard deviation of the population is unknown, the design fractile factor $k_{d,n}$ was calculated using Eq. (14) [61,62]. Note that this may be implemented in Microsoft Excel using Eq. (15).

$$k_{d,n} = -t_p\sqrt{(1+1/n)} \tag{14}$$

$$k_{d,n} = \mathrm{TINV}(2(0.001), n-1)\sqrt{(1+1/n)} \tag{15}$$

The key reliability analysis results are presented in Tables 6 and 7 and Fig. 7, where V_r is given by Eq. (16), γ^*_{M1} is the required value of the partial safety factor and γ_{M1} is the target value of the partial safety factor, equal to 1.1.

$$V_r = \sqrt{V_{rt}^2 + V_\delta^2} \tag{16}$$

The results of each continuous beam load case were split into three sub-groups according to the strain limit of the cross-sections: (1) stocky ($\varepsilon_{csm}/\varepsilon_y \geq 15$), (2) intermediate ($1 \leq \varepsilon_{csm}/\varepsilon_y < 15$) and (3) slender ($\varepsilon_{csm}/\varepsilon_y < 1$); note that in all cases the fractile factor $k_{d,n}$ was based on the total number of tests in the full series [43]. Additionally, to prevent excessively conservative results from skewing the reliability analysis due to the resulting high scatter, the ratio of the benchmark resistance r_e to predicted resistance r_t was capped at 1.3 i.e. $r_e = \min(r_e, 1.3r_t)$.

To satisfy the reliability requirements of [43], the ratio of the required partial safety factor γ^*_{M1} to the target partial safety factor γ_{M1} must be less than or equal to an acceptance limit f_a, defined as [63]:

$$f_a = 1.03 + 0.75(V_r - 0.04) \text{ but } \quad 1.03 \leqslant f_a \leqslant 1.15 \tag{17}$$

Tables 6 and 7 present a summary of the results of the reliability analysis for the continuous beams and frames, respectively. Additionally, Fig. 8 presents a graphical representation of the full results. It can be seen that in all cases the reliability requirements are satisfied, with $\gamma^*_{M1}/\gamma_{M1} \leq f_a$, demonstrating that the proposals can be safely adopted in conjunction with the partial safety factor of 1.1.

6. Worked example

A worked example is presented in this section to illustrate the application of the GMNIA-based design approach with strain limits, as detailed in Section 3. The worked example considers a 6 × 4 m duplex Grade 1.4362 (see Table 2) stainless steel portal frame constructed with rigid joints and fixed supports, as shown in Fig. 9. The frame is fully braced against out-of-plane deformations. The geometric properties and unfactored design loading assumed are included in Fig. 9. Note that centreline dimensions have been used in all the following calculations, with the effects of fillets ignored and a stiffener included at the location of the concentrated load to avoid localised web failure.

As previously discussed, the maximum compressive strains in all cross-sections within the structure must be less than the corresponding CSM strain limits under the factored design loading. For simplicity, the results presented below are only for the critical cross-section (i.e. the cross-section at which the average strains first reach the CSM strain limit in the analysis) in the structure, as identified in Fig. 9.

Step 1a: Calculation of full cross-section local buckling stress.

The full cross-section local buckling stress $\sigma_{cr,cs}$ is calculated using the formulae developed in [11]. For the critical cross-section, the first order elastic stress distribution is shown in Fig. 9. The compression flange is uniformly compressed (i.e. $\psi_f = \sigma_{2,f}/\sigma_{1,f} = 1.0$).Therefore, the buckling coefficients for the isolated outstand flanges with simply-supported k_f^{SS} and fixed k_f^F boundary conditions are $k_f^{SS} = 0.43$ and $k_f^F = 1.25$ [11,39], respectively. For the internal web subjected to combined bending and compression ($\psi_w = \sigma_{2,w}/\sigma_{1,w} = -0.96$), the buckling coefficients are equal to $k_w^{SS} = 22.86$ and $k_w^F = 38.00$. The corresponding elastic critical buckling stresses are: $\sigma_{cr,f}^{SS} = 1670$ MPa, $\sigma_{cr,f}^F = 4855$ MPa, $\sigma_{cr,w}^{SS} = 1954$ MPa, and $\sigma_{cr,w}^F = 3248$ MPa.

The maximum compressive stresses in the flange and web are the same and hence the load correction factors β_f and β_w are equal to unity. The upper and lower bound to the full cross-section local buckling stress $\sigma_{cr,cs}$ are therefore given by:

$$\sigma_{cr,p}^F = \min\left(\beta_f\sigma_{cr,f}^F,\ \beta_w\sigma_{cr,w}^F\right) = 3248 \text{ MPa} \tag{18}$$

Table 7
Summary of statistical analysis results for presented design method assessed against the benchmark shell FE results for austenitic, duplex and ferritic stainless steel I-section portal frames.

Load Case	Grade	b	V_δ	V_r	γ^*_{M1}	$\gamma^*_{M1}/\gamma_{M1}$
F-LC1	Austenitic	0.984	0.046	0.081	1.09	0.99
	Duplex	1.027	0.029	0.051	1.09	0.99
	Ferritic	0.985	0.015	0.068	1.13	1.03
F-LC2	Austenitic	1.055	0.043	0.083	1.04	0.94
	Duplex	1.041	0.020	0.052	1.06	0.96
	Ferritic	1.047	0.033	0.081	1.10	1.00
F-LC3	Austenitic	0.991	0.008	0.070	1.05	0.95
	Duplex	1.002	0.012	0.048	1.09	0.99
	Ferritic	0.994	0.010	0.071	1.12	1.01
F-LC4	Austenitic	0.995	0.014	0.071	1.05	0.96
	Duplex	1.021	0.020	0.050	1.08	0.98
	Ferritic	1.000	0.011	0.070	1.12	1.01
F-LC5	Austenitic	1.011	0.007	0.073	1.03	0.93
	Duplex	1.015	0.007	0.050	1.07	0.97
	Ferritic	1.017	0.010	0.075	1.10	1.00

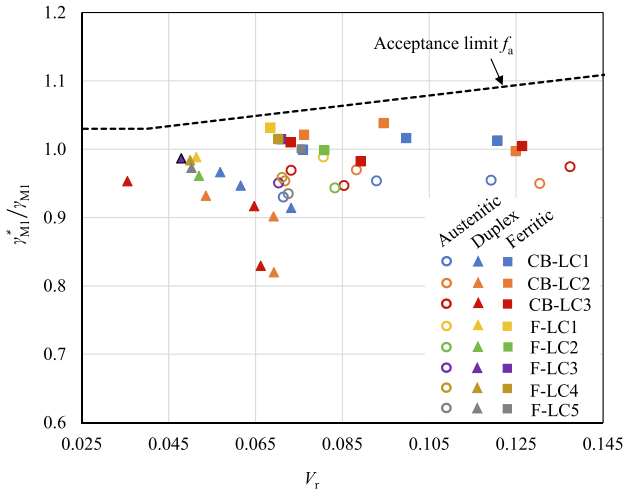


Fig. 8. Comparison of the $\gamma^*_{M1}/\gamma_{M1}$ ratios with the acceptance limit f_a [55] for all load cases considered herein.

$$\sigma^{SS}_{cr,p} = \min\left(\beta_f \sigma^{SS}_{cr,f},\ \beta_w \sigma^{SS}_{cr,w}\right) = 1670 \text{ MPa} \tag{19}$$

The interaction coefficient ζ, accounting for the effects of element interaction, can then be determined from the following expression:

$$\zeta = 0.15\frac{t_f}{t_w}\phi \qquad \text{but} \qquad \zeta \geqslant \frac{t_w}{t_f}(0.4 - 0.25\phi) \tag{20}$$

where $\phi = \sigma^{SS}_{cr,f}/\sigma^{SS}_{cr,w} = 0.86$. Therefore, $\zeta = 0.2013$ and the full cross-section buckling stress $\sigma_{cr,cs}$ at the middle of the beam is given as:

$$\sigma_{cr,cs} = \sigma^{SS}_{cr,p} + \zeta\left(\sigma^{F}_{cr,p} - \sigma^{SS}_{cr,p}\right) = 1670 + 0.2013(3248 - 1670) = 1988 \text{ MPa} \tag{21}$$

Step 1b: Calculation of local cross-section slenderness.

The local cross-section slenderness $\bar{\lambda}_p$ is calculated using Eq. (3). Therefore, for the cross-section under consideration:

$$\bar{\lambda}_p = \sqrt{\frac{f_y}{\sigma_{cr,cs}}} = \sqrt{\frac{450}{1988}} = 0.48 \tag{21}$$

Step 1c: Calculation of elastic local buckling half-wavelength.

The formulae developed by [15] are employed to calculate the elastic local buckling half-wavelength $L_{b,cs}$. For the cross-section under consideration, the upper and lower bound to the cross-section local buckling half-wavelength are $L^{SS}_{b,p} = 433$ mm and $L^{F}_{b,p} = 150$ mm, respectively. Utilising the interaction coefficient ζ determined in Step 1a gives:

$$L_{b,cs} = L^{SS}_{b,p} - \zeta\left(L^{SS}_{b,p} - L^{F}_{b,p}\right) = 433 - 0.2013(433 - 150) = 376 \text{ mm} \tag{22}$$

Step 1d: Calculation of CSM strain limit.

The normalised CSM strain limit is defined by Eqs. (4) and (5) as a function of the local cross-section slenderness $\bar{\lambda}_p$. For the cross-section under consideration, where $\bar{\lambda}_p = 0.48$, the normalised CSM strain limit is therefore given by:

$$\frac{\varepsilon_{csm}}{\varepsilon_y} = \frac{0.25}{\bar{\lambda}_p^{3.6}} + \frac{0.002}{\varepsilon_y} = \frac{0.25}{0.48^{3.6}} + \frac{0.002}{450/191000} = 4.36 \tag{23}$$

Note that ε_{csm} may need to be reduced to $\varepsilon_{csm,V}$ for cross-sections experiencing high shear (i.e. $V_{Ed} > 0.5V_{pl,Rd}$). This adjustment will be made in Step 3 with reference to the shear force which can be directly obtained from the GMNIA results at the considered load level.

Step 2: Beam finite element modelling.

A beam finite element model was developed according to the recommendations in Section 3.2. The columns and beam were discretised into 380 and 582 elements, respectively, resulting in a mesh with an element size of $e_L = 10$ mm. Note that the mesh size was chosen to mirror that used in the benchmark shell model to facilitate comparisons of results; a smaller number of elements could be justified through a mesh convergence study. The material properties for Grade 1.4362 duplex stainless steel were taken as the nominal values given in Table 2 [45,46], while the full stress–strain curve was defined using the two-stage Ramberg–Osgood model. A GMNIA of the frame under the design loading was then carried out with equivalent member imperfections [41] modelled in the shape of a half-sine wave ($e_0 = 19.6$ mm for the beam and $e_0 = 13.1$ mm for the columns). Partial load factors of $\gamma_G = 1.35$ and $\gamma_Q = 1.50$, corresponding to permanent and variable loads, respectively, were used.

Step 3a: Verification of structural resistance using presented design method.

The ultimate resistance determined from the GMNIA R_{GMNIA} is the first to occur of (1) the peak load, after which the load-deformation response decreases or (2) the load at which the average strain across the cross-section elastic local buckling half-wavelength reaches the corresponding CSM limiting strain. Therefore, the extreme fibre compressive strains along each member were extracted and averaged across the corresponding cross-section local buckling half-wavelength. The effect of the restraint against cross-sectional deformations caused by the web stiffener at the midspan of the beam was accounted for by averaging the strains to either side of the stiffener [7].

The averaged strains were then compared with the corresponding strain limit to identify the location of the critical cross-section and the corresponding failure load. In this example, the design shear force V_{Ed} does not exceed $0.5V_{pl,Rd}$ throughout the entire frame before the CSM strain limit is reached and thus no reduction to ε_{csm} is necessary. The CSM strain limit is first reached at the cross-section located at the middle of the beam to the left of the web stiffener (in agreement with the location at which local buckling is observed in the benchmark shell FE model), as indicated in Fig. 10b, at a load factor of 1.13, as shown in Fig. 10a, with a peak following at a load factor of 1.29. Note that a discontinuity in both strain limit and strain is observed at the corners of the frame due to the difference in cross-section between the beam and columns. Additionally, at points of very low bending moment (as observed near the ends of the beam and in the middle of the right column) any small amount of compression dominates the cross-section stress distribution resulting in an increased local slenderness and hence a reduced in strain limit; this phenomenon is most significant for

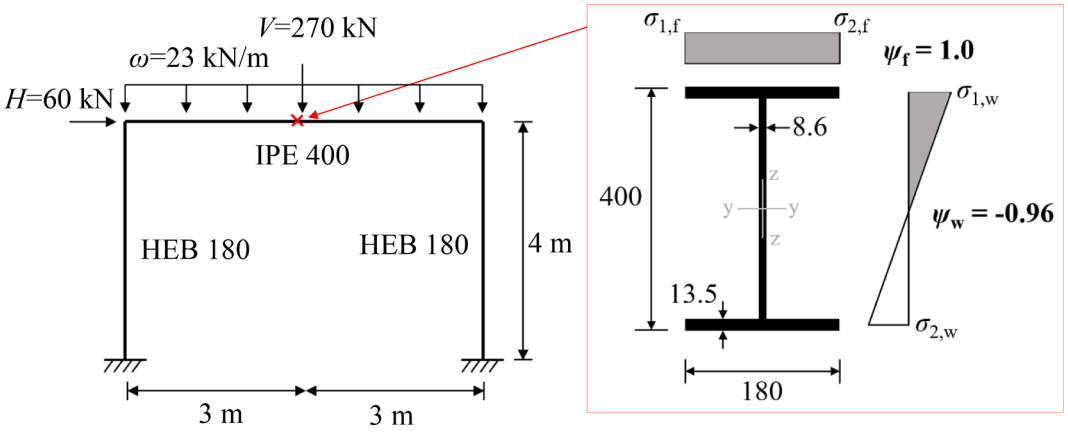


Fig. 9. Geometrical properties and loading condition of the 6 × 4 m frame considered in the worked example, with the first order stress distribution of the critical cross-section, the dimensions of which are shown in mm.

cross-sections with higher aspect ratios h/b where the behaviour of the web is pivotal. However, in such cases, the level of loading is low and thus the cross-sections in question will not be critical. Since the CSM strain limit is reached prior to the attainment of the peak load, the ultimate resistance α_{GMNIA} of the portal frame is governed by the former and $\alpha_{GMNIA} = 1.13$.

Step 3b: Shear check.

The cross-section experiencing the most significant shear throughout the entire frame before failure is located at the end of beam adjacent to the rigid joint, with a design shear force V_{Ed} of 358 kN.

The plastic shear resistance of the IPE 400 beam $V_{pl,Rd}$ is calculated from the following expression assuming $\eta = 1.2$.

$$V_{pl,Rd} = \frac{\eta h_w t_w \left(f_y/\sqrt{3}\right)}{\gamma_{M0}} = \frac{1.2 \times 373 \times 8.6 \times \left(450/\sqrt{3}\right)}{1.1} = 909 \text{ kN} \tag{24}$$

The web of the beam has a slenderness of $\bar{\lambda}_w = 0.72$ and assuming a rigid end post, the shear buckling reduction factor χ_w is equal to 0.95. The shear buckling resistance of the beam $V_{b,Rd}$ is therefore given by:

$$V_{b,Rd} = \chi_w \frac{f_y h_w t_w}{\sqrt{3}\gamma_{M1}} = 0.95 \frac{450 \times 373 \times 8.6}{\sqrt{3} \times 1.1} = 719 \text{ kN} \tag{25}$$

The shear capacity $V_{c,Rd}$ is governed by the lesser of the plastic shear resistance and shear buckling resistance.

$$V_{c,Rd} = \min\left(V_{b,Rd}, V_{pl,Rd}\right) = 719 \text{ kN} \quad \text{and} \quad V_{c,Rd} > V_{Ed} \tag{26}$$

Hence, shear failure is not critical.

Step 4: Verification of resistance against applied loadings.

Finally, the characteristic α_{Rk} and design resistances α_{Rd} can be determined based on the model factor $\gamma_{FE} = 1.0$, as calculated in Section 3.4, and the partial safety factor $\gamma_{M1} = 1.1$:

$$\frac{\alpha_d}{\alpha_{Rd}} = \frac{\alpha_d}{\alpha_{Rk}/\gamma_{M1}} = \frac{\alpha_d}{\alpha_{GMNIA}/(\gamma_{FE}\gamma_{M1})} = \frac{1}{1.13/(1.0 \times 1.1)} = 0.97 < 1.0 \quad \therefore \text{Pass} \tag{27}$$

Fig. 10a shows the response of the portal frame from the GMNIA, where α is the load factor applied to the design loading, as well as the ultimate α_{GMNIA}, characteristic α_{Rk} and design α_{Rd} resistance levels and design load level α_d. Additionally, the corresponding benchmark shell result ($\alpha_{shell} = 1.18$) and Eurocode [42] prediction ($\alpha_{EC3} = 0.88$) according to method M0 (see below) in prEN 1993-1-1 [49] are plotted.

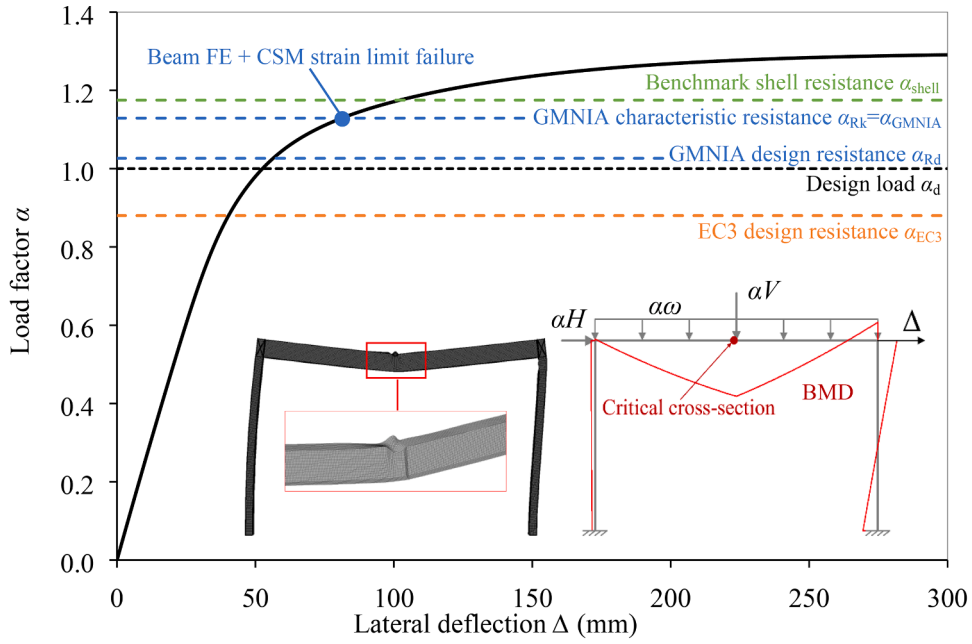
The load amplifiers on the design loads required to achieve the first global sway and member buckling modes are $\alpha_{cr,sw} = 14.0$ and $\alpha_{cr,ns} = 42.3$, respectively. Therefore, the resistance of the frame can be verified according to method M0 in prEN 1993-1-1 [49]. Applying an EN 1993-1-4 [42] linear plastic cross-section check with partial factor $\gamma_{M0} = 1.10$ to the frame based on the results of a linear elastic analysis featuring no imperfection indicates that the cross-sections at both the midspan of the beam and top of the right column would reach a utilisation ratio of 1.0 at a load factor of $\alpha_{EC3} = 0.88$. Therefore:

$$\frac{\alpha_d}{\alpha_{EC3}} = \frac{1}{0.88} = 1.14 > 1.0 \quad \therefore \text{Fail} \tag{28}$$

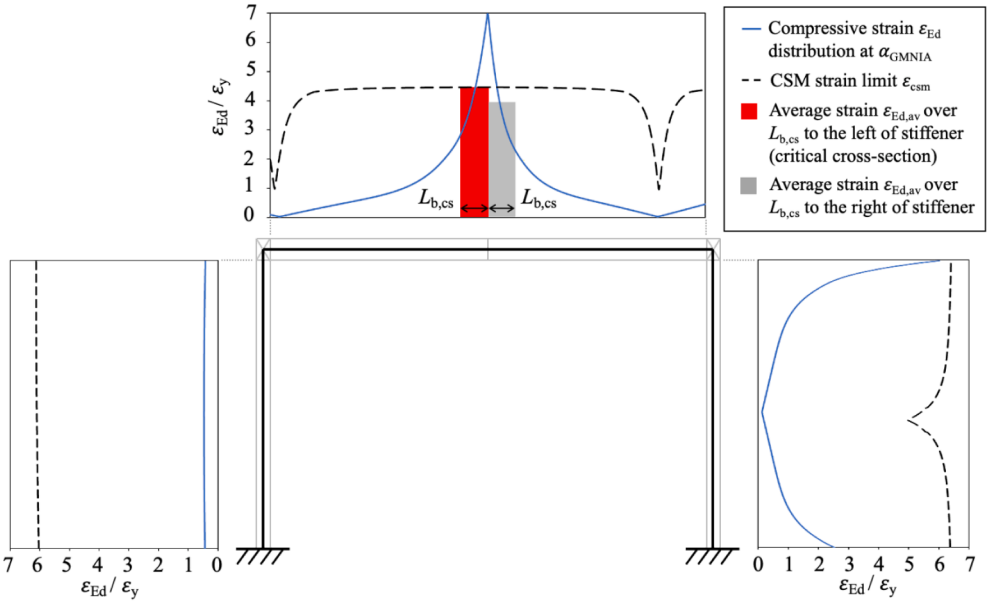
Hence, the frame would fail if its resistance was verified following the traditional design checks set out in prEN 1993-1-4 [42].

7. Conclusions

A recently developed method of design by geometrically and materially nonlinear analysis with imperfections (GMNIA) using beam finite elements and CSM strain limits is presented and extended to stainless steel indeterminate systems. The method is able to capture the beneficial effects of the spread of plasticity, strain hardening, local moment gradients and the degree of permissible moment redistribution due to plastification and member instability. The deformation capacity of cross-sections is considered through the CSM strain limits as a function of the full cross-section slenderness, which eliminate the limitations and overly conservative approximations associated with traditional design methods e.g. step-wise cross-section classification, resistance checks. It is shown that the presented GMNIA-based design method provides consistent capacity predictions for stainless steel indeterminate systems relative to benchmark shell FE results, while providing significant benefits over the traditional Eurocode design methods. A reliability analysis conducted following the provisions of EN 1990 confirmed the suitability of using the existing recommended partial safety factor value of 1.1 in conjunction with the presented design approach. The method is included in AISC 370 and prEN 1993-1-14; inclusion of this design framework in international codes of practice presents a step change for the future direction of structural design.



a) Load-deflection paths and ultimate resistance predictions



b) Strain distribution around the frame at α_{GMNIA} = 1.13

Fig. 10. Worked example: Design of a duplex (f_y = 450 N/mm^2, reduced E = 191000 N/mm^2) stainless steel portal frame, where α is the load factor applied to the design loading.

Declaration of Competing Interest

The authors declare that they have no known competing financial interests or personal relationships that could have appeared to influence the work reported in this paper.

Data availability

Data will be made available on request.

Acknowledgements

The authors would like to acknowledge the funding provided to the second author from the Imperial College London Department of Civil and Environmental Engineering Skempton PhD Scholarship.

References

[1] Liew JYR, Chen WF, Chen H. Advanced inelastic analysis of frame structures. J Constr Steel Res 2000;55:245–65.
[2] Buonopane SG, Schafer BW. Reliability of steel frames designed with advanced analysis. J Struct Eng ASCE 2006;132:267–76.

[3] Gardner L, Yun X, Fieber A, Macorini L. Steel design by advanced analysis: material modeling and strain limits. Engineering 2019;5(2):243–9.
[4] Quan C, Kucukler M, Gardner L. Out-of-plane stability design of steel beams by second-order inelastic analysis with strain limits. Thin-Walled Struct 2021;169:108352.
[5] Gardner, L. 2008. The continuous strength method. Proceedings of the Institution of Civil Engineers - Structures and Buildings, 161: 127–33.
[6] Gardner L, Yun X, Walport F. The Continuous Strength Method - Review and outlook. Eng Struct 2023;275:114924.
[7] Fieber A, Gardner L, Macorini L. Design of structural steel members by advanced inelastic analysis with strain limits. Eng Struct 2019;199:109624.
[8] Fieber A, Gardner L, Macorini L. Structural steel design using second-order inelastic analysis with strain limits. J Constr Steel Res 2020;168:105980.
[9] Walport F, Gardner L, Nethercot DA. Design of structural stainless steel members by second order inelastic analysis with CSM strain limits. Thin-Walled Struct 2021;159:107267.
[10] Quan C, Kucukler M, Gardner L. Design of web-tapered steel I-section members by second-order inelastic analysis with strain limits. Eng Struct 2020;224:111242.
[11] Gardner L, Fieber A, Macorini L. Formulae for calculating elastic local buckling stresses of full structural cross-sections. Structures 2019;17:2–20.
[12] Gardner L. Stability and design of stainless steel structures – Review and outlook. Thin-Walled Struct 2019;141:208–16.
[13] Driscoll Jr GC, Beedle LS. The plastic behavior of structural members and frames. Weld J 1957;36:275-s.
[14] Gioncu V, Petcu D. Available Rotation Capacity of Wide-Flange Beams and Beam-Columns: Part 2. Experimental and Numerical Tests. J Constr Steel Res 1997;43:219–44.
[15] Fieber A, Gardner L, Macorini L. Formulae for determining elastic local buckling half-wavelengths of structural steel cross-sections. J Constr Steel Res 2019;159:493–506.
[16] Baddoo NR, Meza FJ. DG27 - Structural stainless steel design. DG27 2022.
[17] AISC 370. 2021. AISC 370-21: Specification for Structural Stainless Steel Buildings. AISC; 2021.
[18] prEN 1993-1-14. 2021. EN 1993-1-14 – Eurocode 3: Design of steel structures – Part 1-14: Design assisted by finite element analysis Draft.
[19] EN 1993-1-4:2006 + A1: 2015. Eurocode 3 - Design of steel structures - Part 1-4: General rules - Supplementary rules for stainless steels. Brussels: CEN; 2015.
[20] ABAQUS. 2014. Abaqus CAE User's Manual, Version 6.14. Pawtucket, USA: Hibbitt, Karlsson & Sorensen, Inc.; 2014.
[21] Theofanous M, Chan TM, Gardner L. Flexural behaviour of stainless steel oval hollow sections. Thin-Walled Struct 2009;47:776–87.
[22] Bu Y, Gardner L. Finite element modelling and design of welded stainless steel I-section columns. J Constr Steel Res 2019;152:57–67.
[23] Kyvelou P, Gardner L, Nethercot DA. Finite element modelling of composite cold-formed steel flooring systems. Eng Struct 2018;158:28–42.
[24] Kucukler M, Gardner L, Macorini L. Lateral-torsional buckling assessment of steel beams through a stiffness reduction method. J Constr Steel Res 2015;109:87–100.
[25] Kucukler M, Gardner L, Macorini L. A stiffness reduction method for the in-plane design of structural steel elements. Eng Struct 2014;73:72–84.
[26] Rasmussen KJR. Full-range stress–strain curves for stainless steel alloys. J Constr Steel Res 2003;59:47–61.
[27] Mirambell E, Real E. On the calculation of deflections in structural stainless steel beams: an experimental and numerical investigation. J Constr Steel Res 2000;54:109–33.
[28] Arrayago I, Real E, Gardner L. Description of stress-strain curves for stainless steel alloys. Mater Des 2015;87:540–52.
[29] Kucukler M, Xing Z, Gardner L. Behaviour and design of stainless steel I-section columns in fire. J Constr Steel Res 2020;164:105890.
[30] Yuan HX, Wang YQ, Shi YJ, Gardner L. Residual stress distributions in welded stainless steel sections. Thin-Walled Struct 2014;79:38–51.
[31] EN 1090-2. 2018. EN 1090-2 - Execution of steel structures and aluminium structures. Part 2: Technical requirements for steel structures. BSI; 2018.
[32] Walport F, Kucukler M, Gardner L. Stability Design of Stainless Steel Structures. J Struct Eng ASCE 2022;148:04021225.
[33] Kuhlmann, U., Knobloch, M., Lindner, J., Taras, A., Jorg, F., & Bours, A.-L. Neue Entwicklungen in prEN 1993-1-1:2020. In: Kuhlmann U, editor. Stahlbau-Kalender 2020., Berlin: Ernst & Sohn; 2020.
[34] Knobloch M, Bureau A, Kuhlmann U, da Silva LS, Snijder HH, Taras A, et al. Structural member stability verification in the new Part 1–1 of the second generation of Eurocode 3: Part 1: Evolution of Eurocodes, background to partial factors, cross-section classification and structural analysis. Steel Construction 2020;13(2):98–113.
[35] Theofanous M, Saliba N, Zhao O, Gardner L. Ultimate response of stainless steel continuous beams. Thin Walled Struct 2014;83:115–27.
[36] Chen XW, Yuan HX, Du XX, Zhu ZW. Nonlinear deformation behaviour and design of welded stainless steel I-section flexural members. Eng Struct 2022;252:113683.
[37] Yun X, Gardner L, Boissonnade N. The continuous strength method for the design of hot-rolled steel cross-sections. Eng Struct 2018;157:179–91.
[38] EN 1993-1-1. 2005. Eurocode 3: Design of steel structures - Part 1-1: General rules and rules for buildings. Brussels: CEN; 2005.
[39] EN 1993-1-5. 2009. Eurocode 3 - Design of steel structures - Part 1-5 : Plated structural elements. Brussels: CEN; 2009.
[40] Li, Z., & Schafer, B.W. 2010. Buckling analysis of cold-formed steel members with general boundary conditions using CUFSM: Conventional and constrained finite strip methods. Proceedings Twentieth International Specialty Conference on Cold-Formed Steel Structures,: 17–31.
[41] Walport F, Gardner L, Nethercot DA. Equivalent bow imperfections for use in design by second order inelastic analysis. Structures 2020;26:670–85.
[42] prEN 1993-1-4. 2020. Eurocode 3 - Design of steel structures - Part 1-4: General rules - Supplementary rules for stainless steels. CEN, Draft 2.
[43] EN 1990. 2002. Eurocode - Basis of structural design. Brussels: CEN; 2002.
[44] Baddoo NR. Stainless steel in construction: A review of research, applications, challenges and opportunities. J Constr Steel Res 2008;64:1199–206.
[45] EN10088. 2014. BSI Standards Publication Stainless steels Part 3 : Technical delivery conditions for sections and bright products of corrosion.
[46] Afshan S, Zhao O, Gardner L. Standardised material properties for numerical parametric studies of stainless steel structures and buckling curves for tubular columns. J Constr Steel Res 2019;152:2–11.
[47] Kyvelou P, Hui C, Gardner L, Nethercot DA. Moment redistribution in cold-formed steel sleeved and overlapped two-span purlin systems. Adv Struct Eng 2018;21:2534–52.
[48] Kyvelou P, Nethercot DA, Hadjipantelis N, Kyprianou C, Gardner L. The evolving basis for the design of light gauge steel systems. Int J Struct Stab Dyn 2020;20:2041008.
[49] prEN 1993-1-1. 2020. Eurocode 3 – Design of steel structures – Part 1-1: General rules and rules for buildings. CEN,: Final Draft.
[50] Zhang H, Ellingwood BR, Rasmussen KJR. System reliabilities in steel structural frame design by inelastic analysis. Eng Struct 2014;81:341–8.
[51] Liu W, Zhang H, Rasmussen K. System reliability-based Direct Design Method for space frames with cold–formed steel hollow sections. Eng Struct 2018;166:79–92.
[52] Liu W, Zhang H, Rasmussen KJR, Yan S. System-based limit state design criterion for 3D steel frames under wind loads. J Constr Steel Res 2019;157:440–9.
[53] Sena Cardoso F, Zhang H, Rasmussen KJR. System reliability-based criteria for the design of steel storage rack frames by advanced analysis: Part II – Reliability analysis and design applications. Thin-Walled Struct 2019;141:725–39.
[54] Thai HT, Uy B, Kang WH, Hicks S. System reliability evaluation of steel frames with semi-rigid connections. J Constr Steel Res 2016;121:29–39.
[55] Zhang H, Shayan S, Rasmussen KJR, Ellingwood B. System-based design of planar steel frames, I: Reliability framework. J Constr Steel Res 2016;123:135–43.
[56] Arrayago I, Rasmussen KJR. System-based reliability analysis of stainless steel frames under gravity loads. Eng Struct 2021;231:111775.
[57] Arrayago I, Rasmussen KJR, Zhang H. System-based reliability analysis of stainless steel frames subjected to gravity and wind loads. Struct Saf 2022;97:102211.
[58] Afshan S, Francis P, Baddoo NR, Gardner L. Reliability analysis of structural stainless steel design provisions. J Constr Steel Res 2015;114:293–304.
[59] Meng X, Gardner L. Stability and design of normal and high strength steel CHS beam-columns. Eng Struct 2022;251:113361.
[60] Meng X, Gardner L, Sadowski AJ, Rotter JM. Elasto-plastic behaviour and design of semi-compact circular hollow sections. Thin-Walled Struct 2020;148:106486.
[61] Kang WH, Hicks SJ, Uy B, Fussell A. Design resistance evaluation for steel and steel-concrete composite members. J Constr Steel Res 2018;147:523–48.
[62] Tankova T, Simões Da Silva L, Marques L, Rebelo C, Taras A. Towards a standardized procedure for the safety assessment of stability design rules. J Constr Steel Res 2014;103:290–302.
[63] SAFEBRICTILE. 2016. Standardization of safety assessment procedures across brittle to ductile failure modes. Grant Agreement Number: RFSR-CT-2013-00023, Deliverable D11 - Guideline for the Safety Assessment of Design Rules for Steel Structures in Line with EN 1990.